Applied Physics Letters

Separative extended-gate AlGaAs/GaAs HEMT biosensors based on capacitance change strategy

Cite as: Appl. Phys. Lett. **116**, 123704 (2020); https://doi.org/10.1063/5.0001786
Submitted: 21 January 2020 . Accepted: 11 March 2020 . Published Online: 24 March 2020

Jiahuan Yu, Mengke Xu, Lingyan Liang, Min Guan, Yang Zhang, Feng Yan, and Hongtao Cao

Applied Physics Letters ARTICLE scitation.org/journal/apl

Separative extended-gate AlGaAs/GaAs HEMT biosensors based on capacitance change strategy

Cite as: Appl. Phys. Lett. **116**, 123704 (2020); doi: 10.1063/5.0001786
Submitted: 21 January 2020 · Accepted: 11 March 2020 ·
Published Online: 24 March 2020

Jiahuan Yu,[1,2] Mengke Xu,[2,3] Lingyan Liang,[1,a)] Min Guan,[3,a)] Yang Zhang,[3,a)] Feng Yan,[4] and Hongtao Cao[1,2]

AFFILIATIONS

[1]Division of Functional Materials and Nano Devices, Ningbo Institute of Materials Technology and Engineering, Chinese Academy of Sciences, Ningbo 315201, People's Republic of China
[2]Center of Materials Science and Optoelectronics Engineering, University of Chinese Academy of Sciences, Beijing 100049, People's Republic of China
[3]Key Laboratory of Semiconductor Material Sciences, Beijing Key Laboratory of Low Dimensional Semiconductor Materials and Devices, Institute of Semiconductors, Chinese Academy of Sciences, Beijing 100083, People's Republic of China
[4]Department of Applied Physics, The Hong Kong Polytechnic University, Hung Hom, Kowloon, Hong Kong

[a)]**Authors to whom correspondence should be addressed:** lly@nimte.ac.cn; guanmin@semi.ac.cn; and zhang_yang@semi.ac.cn

ABSTRACT

Separative extended-gate AlGaAs/GaAs high electron mobility transistor (HEMT) biosensors based on the capacitance change strategy are proposed and fabricated. The working mechanism underlying this strategy is clearly clarified via examining the capacitance evolution on biorecognition and the capacitance matching issue between the HEMT and the sensing pad. The fabricated biosensors demonstrate a good linear current/voltage response to a label-free prostate-specific antigen (PSA) target over a broad concentration range of 100 fg/ml to 10 ng/ml in both 0.1× and 1× phosphate buffered saline solutions. Specifically, the sensitivity variation approaches 8.7% dec^{-1} at the critical concentration level of 2–8 ng/ml that enters the normal PSA region in the human body. The advantages of high sensitivity, low-cost, and convenience of usage make the proposed HEMT biosensors potential candidates for prostate cancer diagnosis.

Bioelectronics, which provides a bridge between biology and electronics, has gained leap-forward development during the past ten years.[1–3] Field effect transistors (FETs), one of the basic semiconductor devices, have demonstrated a vast array of biosensing applications due to their inherent amplification function, high degree of openness, and integration compatibility with other electronic/optoelectronic systems.[4–6] High electron mobility transistors (HEMTs) as special kinds of FETs, featuring high transconductance and low noise, are regarded as promising candidates for biosensors with high sensitivity and reliability.[7–9] However, in early reports, the gate electrode at the top of the HEMTs was often chosen as the sensing element;[7,10] therefore, the HEMTs with relatively high manufacturing costs would inevitably come into contact with various biological solutions and, thus, their service life would be severely limited. Then, an extended-gate[7]/floating-gate[11] sensing pad was proposed to keep the HEMT devices away from the biological solutions, but this scheme was not very effective. The separative extended-gate configuration is thought to be capable of solving the solution erosion issue during the biomodification and biosensing processes because this design provides high independence between the transistor and the sensing pad in terms of fabrication/measurement conditions and substrates used. Although the separative extended-gate configuration has been used in biosensors based on MOSFETs,[12] thin-film transistors,[13] nanowire FETs,[14,15] etc., it has been rarely reported in HEMT-based biosensors.[16]

To meet the demand of specific analyte detection, much effort was made to develop bioelectronic devices with various working mechanisms, including surface potential,[17] electrochemical reaction induced charge redistribution,[18] or capacitance change[19] due to biorecognition. Among them, the surface potential change was frequently used, but the corresponding biosensors always suffered from low sensitivity due to the charge screen effect, especially in high ion concentration solutions.[20] The electrochemical reaction and capacitance change strategy were also investigated, demonstrating well-performed sensitivity and the low detection limit.[21] But, nevertheless, the electrochemical reaction strategy involves relatively complex surface modification with electrochemically active components,[22] while the capacitance change strategy does not use complex surface modification but refers to the capacitance matching issue, which needs further investigation.

Prostate cancer is an epithelial malignancy that occurs in the prostate gland and ranks the sixth in the incidence of male malignancy. Prostate-specific antigen (PSA), as the preferred biomarker for the diagnosis of prostate cancer,[23] is a protein secreted by prostate cells and present in healthy people at a very low level. In this study, based on the capacitance change strategy, we fabricated separative extended-gate AlGaAs/GaAs HEMT biosensors with a sensing pad on cheap glass to detect PSA. A good linear relation between the threshold voltage shift (sensitivity) and the logarithm of PSA antigen concentration was achieved in both 0.1× and 1× phosphate buffered saline (PBS) solutions. The maximum sensitivity is up to 55% for 10 ng/ml PSA in 0.1× PBS solution. The related sensing properties are well explained in terms of the capacitance change due to biorecognition, as well as the capacitance matching between the HEMT device and the sensing pad with electrical double layer (EDL) capacitance.

High performance HEMT devices were fabricated on GaAs substrates. As shown in Fig. 1(a), the AlGaAs/GaAs epitaxy–wafer, consisting of a 2 μm-GaAs Buffer layer, a 12 nm InGaAs channel layer, a 28 nm AlGaAs barrier layer, and a 30 nm GaAs cap layer, was produced using Molecular Beam Epitaxy (MBE). The electrical resistivity of the HEMT was 388.3 Ω cm, and the sheet electron concentration was $1.9 \times 10^{12}\,\mathrm{cm}^{-3}$ with a mobility of $8.5 \times 10^{3}\ \mathrm{cm}^{2}\mathrm{V}^{-1}\mathrm{s}^{-1}$. The preparation details are given in the supplementary material. The preparing process of the separative sensing pad is schematically shown in Fig. 1(b). First, 40 nm Ti and 60 nm Au were deposited in sequence on a glass substrate by electron beam evaporation, yielding a pair of gold electrodes with an interval space of 1 mm via a shadow mask. One of them (with an area of $5 \times 7\ \mathrm{mm}^2$) was selected as the biomodification region, and the modification process is described in the supplementary material. After finishing the modification, the sensing pad was connected to the HEMT device by a conductive fiber to form a separative extended-EDL-gate HEMT biosensor, as shown in Fig. 1(c). When 12 μl of PSA solution was added dropwise on the sensor, the solution would bridge the gold electrode pair. Herein, it should be noted that the probe cannot touch the solution, in order to avoid the reaction between the solution and the probe when the gate bias is applied. The device electrical properties were characterized using a Keithley-4200 SCS semiconductor parameter analyzer at room temperature in the dark. In this study, the electrical measurements were carried out for probing PSA antigen in 0.1× and 1× PBS solutions.

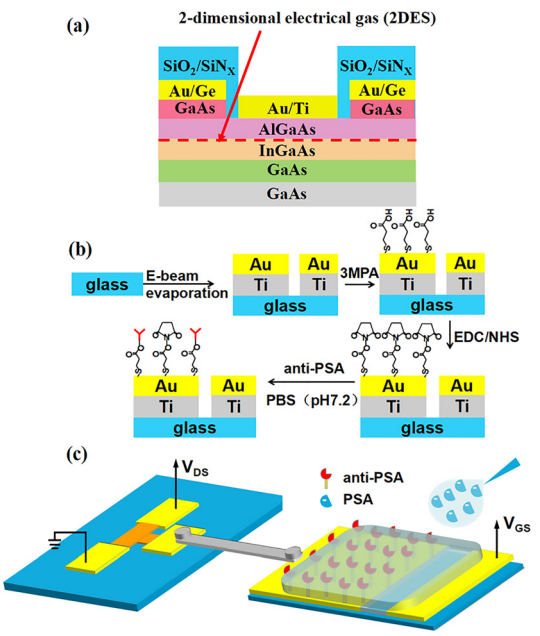

FIG. 1. Schematic diagram of the AlGaAs/GaAs HEMT structure (a), the modification process of the sensing pad (b), and the separative extended-EDL-gate HEMT biosensor (c).

Figure 2(a) shows the typical transfer curves of the separative extended-gate HEMT biosensor probing PSA with different concentrations (in 0.1× PBS) at a fixed source-drain voltage of 0.1 V. It can be observed that the transfer curves demonstrate a successive and positive shift as the PSA concentration ([PSA]) increases from 100 fg/ml to 10 ng/ml. When the PSA concentration is lower than 100 fg/ml, the transfer curve shift is negligible, indicating that the limit of detection (LOD) of our sensors is about ~100 fg/ml. The threshold voltage (V_{TH}) is estimated from the voltage intercept by extrapolating the linear portion of the source-drain current (I_{DS}) vs gate voltage (V_{GS}) curve to $I_{DS} = 0$, as illustrated in Fig. 2(a). The threshold voltage change (ΔV_{TH}) relative to the pure PBS's case is derived and shown in Fig. 2(b) as a function of PSA concentration on a logarithmic scale. A good linearity can be clearly observed with an R^2 value (R is the correlation coefficient) of ~0.99. The ΔV_{TH} value of each concentration was about 14.5 mV dec^{-1}. In addition, five biosensors are summarized with relatively small error bars, indicating a repeatable sensor response. To prove that the V_{TH} shift stems from the reaction between PSA and anti-PSA, a sensing pad without anti-PSA was also connected to the same HEMT device, and the results are plotted in Fig. 2(b), where the corresponding ΔV_{TH} is changed not only weakly but also chaotically with the increase in [PSA]. In addition, to check the sensing specificity, the fabricated PSA biosensor is also applied to detect other biomolecules. MiR-208a is selected as the biological interference that can be used for the diagnosis of coronary heart disease. As expected, a negligible response to miR-208a was observed, as shown in Fig. 2(b). It should be noted that the high-cost

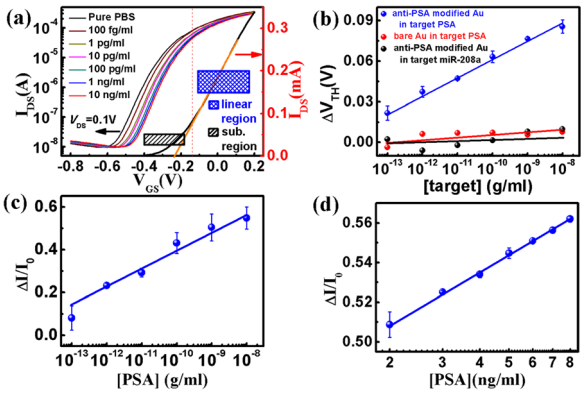

FIG. 2. (a) The logarithmic I_{DS}-V_{GS} curves of the HEMT biosensor at different concentrations of PSA (left) and typical linear I_{DS}-V_{GS} curve for pure PBS (right). ΔV_{TH} (b) and sensitivity (c) at different concentrations of PSA in 0.1× PBS solution. (d) The sensitivity in the concentration range of 2 ng/ml to 8 ng/ml in 0.1× PBS solution.

HEMT component is recyclable in our system although the sensing pad is not. So, in the future, the separative sensing pad can be delicately designed with a plug-in-card-type structure since it is capable of functionalizing various receptor molecules according to different bio-sensing tasks.

The sensitivity is one of the important parameters to evaluate the biosensor performance. In some reports, the absolute change in current (ΔI) measured from the device was defined as the metric, which may lead to device-to-device variations.[24,25] Thus, the sensitivity is preferred to be defined as $S = |\Delta I/I_0| \times 100\%$ (where ΔI is the change in I_{DS} and I_0 is the initial current).[26] The S values of our biosensor are derived based on the transfer curves at a fixed V_{GS} value of -0.14 V at which the FET-sensors are operated in the linear regime and the current change is proportional to the gate voltage. As expected, a linear relation between S and log([PSA]) is manifested in Fig. 2(c), presenting a good linearity with $R^2 = 0.95$. The sensitivity for 10 ng/ml PSA is ~55%, higher than the previously reported results (< 10%).[27–29] Specifically, the sensitivity variation is about 8.45% dec^{-1} as the PSA concentration changes tenfold within the range of 10 ng/ml to 100 fg/ml. Therefore, our device can distinguish target biomolecules with a small concentration change.

In general, the normal level of PSA in the human body is less than 4 ng/ml,[26] and hence, it is highly desirable to achieve a biosensor that can distinguish the PSA around this critical value. The separative extended-gate HEMT biosensor was used to detect PSA from 2 to 8 ng/ml in 0.1× PBS. As shown in Fig. 2(d), the S vs log([PSA]) plot shows a good linearity with $R^2 \sim 0.99$. Similar to the above-mentioned case (8.45% dec^{-1}, from 10 ng/ml to 100 fg/ml), the sensitivity variation is ~8.7% dec^{-1} within the scope ranging from 2 to 8 ng/ml, indicating good discrimination in this critical range.

The above results demonstrate that the HEMT biosensor reported here has a well-performed detection capability. The inherent reason is closely related to the capacitance change. As shown in Fig. 3(a), the mobile ions in the solution will migrate under the electric field and form an EDL on each of the electrodes when the gate bias is applied on the sensing pad. In this case, a solution EDL capacitance (C_s) is formed in series with the HEMT device capacitance (C_d). Thus, the potential drop across the transistor (V_d) can be expressed by[30]

$$V_d = \frac{C_s}{C_d + C_s} V_g. \quad (1)$$

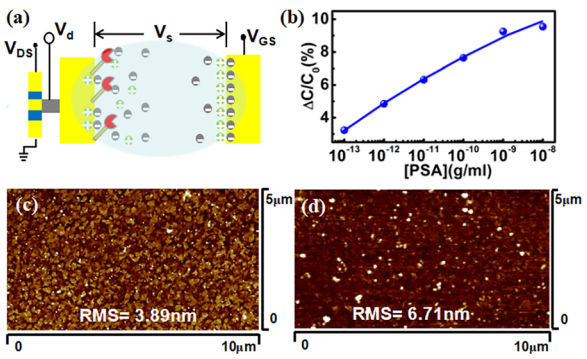

FIG. 3. (a) Schematic illustration of EDL formation. (b) The C_s changes at different concentrations of PSA in 0.1× PBS solution. AFM images of anti-PSA modified (c) and PSA (100 pg/ml)/anti PSA (d) modified surfaces.

It is inferred that C_s can effectively modulate V_d and consequently I_{DS} if C_d is larger than or comparable to C_s. The C_s value (at 20 Hz) is obtained to be near 1 μF in pure 0.1× PBS by directly measuring the capacitance between the electrode pair, while C_d between the gate and source/drain electrodes exceeds 100 μF at low frequency when the HEMT is turned on (Fig. S1). Such a large C_d value benefits from the design of a direct contact between the gate electrode and AlGaAs barrier layers. In this case, Eq. (1) can be simplified by $V_d \approx C_s/C_d \times V_g$, meaning that the variations of V_d (I_{DS} in turn) are closely coupled with C_s in our HEMT biosensors. Figure 3(b) displays the capacitance changes ($\Delta C/C_0$, where ΔC is the difference between the EDL capacitance measured in PBS + PSA solution and C_0 the capacitance in pure 0.1× PBS) as a function of [PSA]. $\Delta C/C_0$ demonstrates a near-linear increase with [PSA], up to 9.54% for 10 ng/ml PSA. This indicates that the binding of the antibody and antigen can change C_s effectively. It has been reported that the charge density of many biomolecules (such as dsDNA) is at least one order of magnitude higher than physiological salt concentrations.[31,32] So it is believed that the spatial distribution of anti-PSA and PSA can affect the ionic strength in the local region of the EDL and then C_s to some extent. Atomic force microscopy (AFM) images illustrate that the surface morphology has been changed obviously after the binding of PSA to anti-PSA [Figs. 3(c) and 3(d)]. In addition, the charged biomolecule bending or movement under the electrical field in solution may also contribute to the C_s change, which needs further investigation such as simulation of molecular dynamics.[28]

Furthermore, considering the high sensitivity in 0.1× PBS, the HEMT biosensors were also applied to probe the PSA antigen in 1× PBS, which is of practical significance since the ion concentration of 1× PBS is much closer to human serum. In general, the detection of biomolecules in 0.1× PBS was frequently investigated in the literature, because high ion concentration solution has a serious charge screen effect, which would limit the probing sensitivity. But, fortunately, our HEMT biosensors still have a relatively acceptable detection capability in the 1× PBS solution. As seen in Fig. 4(a), ΔV_{TH} presents a good linear relationship ($R^2 = 0.99$) as a function of the logarithm of PSA concentration ranging from 100 fg/ml to 10 ng/ml, with a sensitivity variation of about 8.9 mV dec^{-1}. In addition, the linear fitting curve has a logarithmic sensitivity as a function of [PSA], where $R^2 = 0.98$ [Fig. 4(b)]. Although these major sensing parameters in 1× PBS are inferior to those in 0.1× PBS, the character parameters reported here are comparable/superior to the previously reported results in 0.1× PBS,[27–29] demonstrating a good potential application for direct protein detection in physiological environments.

In conclusion, separative extended-gate AlGaAs/GaAs HEMT biosensors based on the capacitance change strategy were designed and fabricated to detect the PSA. Both the threshold voltage shift and the sensitivity have good linear relationships with the logarithm of PSA concentration ranging from 100 fg/ml to 10 ng/ml in both 0.1× and 1× PBS solutions. The maximum sensitivity is up to 55% and 35% for 10 ng/ml PSA in 0.1× and 1× PBS solutions, respectively. Additionally, the sensors also demonstrate a good discrimination in a narrow range (2–8 ng/ml) around the normal level of PSA in the human body. With the excellent electrical properties and the potential for plug-in-card-type multifunctional sensing, the proposed biosensors would be promising candidates for the development of portable biosensors for public health applications.

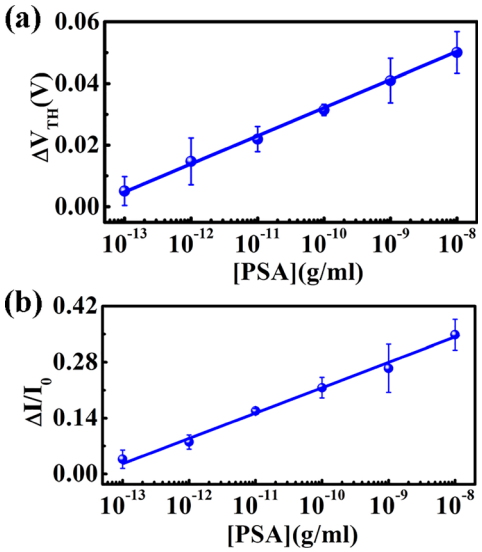

FIG. 4. ΔV_{TH} (a) and sensitivity (b) for different concentrations of PSA in 1× PBS solution.

See the supplementary material for the procedure of HEMT preparation and biological modification, the capacitance of HEMT, and the solution EDL capacitance of the separative sensing pad.

This work was supported by the National Natural Science Foundation of China (No. 61874105), the Natural Science Foundation of Zhejiang Province (No. LY20F010002), the Program for Ningbo Municipal Science and Technology Innovative Research Team (Grant No. 2016B10005), and the Natural Science Foundation of Ningbo (2018A610038).

REFERENCES

[1]M. Shinwar, M. Deen, and D. Landheer, Microelectron. Rel. **47**, 2025–2057 (2007).
[2]D.-S. Kim, J.-E. Park, J.-K. Shin, P. Kim, G. Lim, and S. S. Park, Sens. Actuators, B **117**, 488–494 (2006).
[3]S. Meyburg, M. Goryll, J. Moers, S. Ingebrandt, S. Bocker-Meffert, H. Luth, and A. Offenhausser, Biosens. Bioelectron. **21**, 1037–1044 (2006).
[4]S. S. Cheng, S. Hideshima, S. Kuroiwa, T. Nakanishi, and T. Osaka, Sens. Actuators, B **212**, 329–334 (2015).
[5]T. Sakata and Y. Miyahara, Biosens. Bioelectron. **21**(5), 827–832 (2005).
[6]T. Sakata, M. Kamahori, and Y. Miyahara, Jpn. J. Appl. Phys., Part 1 **44**(4B), 2854–2859 (2005).
[7]K. Ding, C. Y. Wang, B. Zhang, Y. Zhang, M. Guan, L. J. Cui, Y. W. Zhang, Y. P. Zeng, Z. Lin, and F. Huang, IEEE Electron Device Lett. **35**(3), 333–335 (2014).
[8]Y. L. Wang, B. H. Chu, K. H. Chen, C. Y. Chang, T. P. Lele, Y. Tseng, S. J. Pearton, J. Ramage, D. Hooten, A. Dabiran, P. P. Chow, and F. Ren, Appl. Phys. Lett. **93**(26), 262101 (2008).
[9]B. H. Chu, C. Y. Chang, K. Kroll, N. Denslow, Y. L. Wang, S. J. Pearton, A. M. Dabiran, A. M. Wowchak, B. Cui, P. P. Chow, and F. Ren, Appl. Phys. Lett. **96**(1), 013701 (2010).
[10]J. Lee, L. G. Kaake, J. H. Cho, X. Y. Zhu, T. P. Lodge, and C. D. Frisbie, J. Chem. Phys. **113**(20), 8972–8981 (2009).
[11]F. S. Tulip, E. Eteshola, S. Desai, S. Mostafa, S. Roopa, B. Evans, and S. K. Islam, IEEE Trans. Nanobioscience **13**(2), 138–145 (2014).
[12]J. Choi, H. H. Lee, J. Ahn, S. H. Seo, and J. K. Shin, Jpn. J. Appl. Phys., Part 1 **51**(6), SI06FG05 (2012).
[13]L. Y. Liang, S. N. Zhang, W. H. Wu, L. Q. Zhu, H. Xiao, Y. H. Liu, H. L. Zhang, K. Javaid, and H. T. Cao, Appl. Phys. Lett. **109**(17), 173501 (2016).
[14]C. W. Chen, R. Z. Lin, L. C. Chiang, F. M. Pan, and J. T. Sheu, Jpn. J. Appl. Phys., Part 1 **58**(2), 027001 (2019).
[15]C. P. Chen, A. Ganguly, C. Y. Lu, T. Y. Chen, C. C. Kuo, R. S. Chen, W. H. Tu, W. B. Fischer, K. H. Chen, and L. C. Chen, Anal. Chem. **83**(6), 1938–1943 (2011).
[16]S. Yang, L. Gu, X. Z. Ding, B. Miao, Z. Q. Gu, L. Y. Yang, J. D. Li, and D. M. Wu, IEEE Electron Device Lett. **39**(10), 1592–1595 (2018).
[17]L. Herlogsson, X. Crispin, N. D. Robinson, M. Sandberg, O. Hagel, G. Gustafsson, and M. Berggren, Adv. Mater. **19**(1), 97 (2007).
[18]F. Yan, M. Zhang, and J. H. Li, Adv. Healthcare Mater. **3**(3), 313–331 (2014).
[19]X. Guo, J. Liu, F. Liu, F. She, Q. Zheng, H. Tang, M. Ma, and S. Yao, Sens. Actuators, B **240**, 1075–1082 (2017).
[20]N. Gao, W. Zhou, X. C. Jiang, G. S. Hong, T. M. Fu, and C. M. Lieber, Nano Lett. **15**(3), 2143–2148 (2015).
[21]N. X. Wang, A. N. Yang, Y. Fu, Y. Z. Li, and F. Yan, Acc. Chem. Res. **52**(2), 277–287 (2019).
[22]Y. Fu, N. X. Wang, A. N. Yang, H. K. Law, L. Li, and F. Yan, Adv. Mater. **29**(41), 1703787 (2017).
[23]P. R. Carroll, J. M. Whitson, and M. R. Cooperberg, J. Clin. Oncol. **29**(4), 345–347 (2011).
[24]B. M. Lowe, K. Sun, I. Zeimpekis, C.-K. Skylaris, and N. G. Green, Analyst **142**(22), 4173–4200 (2017).
[25]F. N. Ishikawa, M. Curreli, H.-K. Chang, P.-C. Chen, R. Zhang, R. J. Cote, M. E. Thompson, and C. W. Zhou, ACS Nano **3**(12), 3969–3976 (2009).
[26]L. L. Wang, J. A. Jackman, W. B. Ng, and N.-J. Cho, Adv. Funct. Mater. **26**(47), 8623–8630 (2016).
[27]J. D. Li, J. J. Cheng, B. Miao, X. W. Wei, J. Xie, J. C. Zhang, Z. Q. Zhang, H. W. Li, and D. M. Wu, Microsyst. Technol. **21**(7), 1489–1494 (2015).
[28]Z. Q. Gu, J. Wang, B. Miao, L. Zhao, X. S. Liu, D. M. Wu, and J. D. Li, RSC Adv. **9**(27), 15341–15349 (2019).
[29]J. D. Li, J. J. Cheng, B. Miao, X. W. Wei, J. Xie, J. C. Zhang, Z. Q. Zhang, and D. M. Wu, J. Micromech. Microeng. **24**(7), 075023 (2014).
[30]C. H. Chu, I. Sarangadharan, A. Regmi, Y. W. Chen, C. P. Hsu, W. H. Chang, G. Y. Lee, J. I. Chyi, C. C. Chen, S. C. Shiesh, G. B. Lee, and Y. L. Wang, Sci. Rep. **7**, 5256 (2017).
[31]H. Long, A. Kudlay, and G. C. Schatz, J. Phys. Chem. B **110**(6), 2918–2926 (2006).
[32]C. P. Hsu, Y. F. Huang, and Y. L. Wang, ECS J. Solid State Sci. Technol. **5**(6), Q149–Q154 (2016).